Numerical Modelling of Induction Heating of Long Workpieces

C. Chaboudez, S. Clain, R. Glardon, J. Rappaz, M. Swierkosz and R. Touzani

Abstract—**We consider in this paper an induction heating process. A mathematical model is presented, together with numerical methods used in order to describe the magnetic field, as well as the temperature field evolution. Experimental measurements were performed in order to validate the numerical simulation results. A comparison is presented for both ferromagnetic and non-ferromagnetic materials. An error discussion is provided.**

I. Introduction

THE induction heating process is widely used in industrial operations like metal hardening, preheating for forging operations or brasing [2]. It consists in generating heat by means of the Joule effect resulting from an eddy current. Despite the apparent simplicity of this description, induction heating is a complex phenomenon. Therefore, the design of an induction heating system can be tedious and often relies upon an experimentally based trial and error process. Furthermore, temperature measurements inside workpieces are expensive and time-consuming. As they do not provide much general information about the process, they must be repeated for every single heating case. Moreover, precise temperature measurements are difficult to perform, and introducing temperature sensors into the induction heating setup often results in perturbating the phenomenon.

Therefore, numerical simulation seems a well-adapted tool for the design and the investigation of induction heating systems. Thanks to the progress accomplished these last years in computer technology, it is now possible to efficiently handle several cases of induction heating in a short time, and a modification of the experimental parameters implies very little additional work. This allows for a considerable reduction of the time and design costs required for the development of an induction heating unit, since much of the experimental work can be replaced by computer simulation. Although eddy currents computation is the subject of many articles (e.g. [6]–[8]), numerical simulation of induction heating has not been extensively described in the literature, and most of the authors limit their scope to induction heating systems with simple geometries [4], [9]–[19].

Our research, conducted at the Department of Mathematics of the Federal Institute of Technology in Lausanne, Switzerland in collaboration with the company AMYSA Yverdon S.A., and financed by the Swiss National Energy Research Fund (NEFF) aims at elaborating mathematical and numerical models, and constructing efficient numerical codes for the simulation of induction heating.

We have first dealt with the situation when the induction heating setup (coil and heated workpieces) is long and has a constant cross-section. The mathematical model obtained in this case is not exceedingly intricated, yet the numerical code based on this model yields valuable results, as will be shown in the sequel. It deals with both ferromagnetic and non-ferromagnetic materials, the physical properties of which may vary both with the temperature and with the magnetic field. It also can handle non-sinusoidal currents, which are widely used in industrial applications. The results given by the code have been compared with experimental measurements performed by the company AMYSA Yverdon S.A. This comparison gave very good results.

In this note, we will briefly present our model and numerical methods implemented in the code. Then, we will describe the induction heating setup used for in-situ measurements. Finally, comparisons between numerical simulation and in-situ experiments will be presented.

II. Numerical Simulation: Mathematical Model and Numerical Methods

A. The Model

As stated above, we deal with the situation when the induction heating setup has a constant cross-section, the dimensions of which are small compared to the setup length. Practically, our model gives consistent results in the central part of the workpiece (i.e., far from its ends) when the length of the setup is at least four times larger than the diameter of the workpiece, and the precision of the results increases when this proportion grows bigger. These conditions on the dimension of the setup allow us to use the assumption that the magnetic field is orthogonal to the setup cross-section. The mathematical description of the magnetic field is then considerably simplified. A detailed description of the model can be found in [1].

Manuscript received September 19, 1993; revised January 14, 1994. This work was supported by the Swiss "Nationaler Energie-Forschungs-Fonds."

C. Chaboudez and R. Glardon are with Amysa-Yverdon S.A, Route de Lausanne 10, 1400 Yverdon-les-Bains, Switzerland.

S. Clain, J. Rappaz, M. Swierkosz, and R. Touzani are with the Department of Mathematics, Swiss Federal Institute of Technology, 1015 Lausanne, Switzerland.

IEEE Log Number 9403997.

Consider a setup consisting of a coil and of one or several workpieces. We consider that the physical properties of the materials, namely the magnetic permeability μ, the electric conductivity σ, the thermal conductivity λ, the density ρ and the specific heat C_p depend on the temperature. They also depend on the spatial coordinates, since the workpieces and the coil may consist of different materials. Moreover, in the case of ferromagnetic materials, the magnetic permeability μ depends also on the local value of the magnetic field **H**. However, hysteresis loops will not be taken into account, and we will replace them (like in [3], [4], [5]) by a single valued, possibly nonlinear, dependence of μ on **H**. The voltage in the circuit will be prescribed, rather than the total current. This choice was motivated by the fact that the voltage is better controlled than the total current, due to the used generator technology. Typically, the currents involved are periodic (not necessarily sinusoidal), with a frequency of the order of 10 000 Hz. Displacement currents will be neglected.

Our assumptions imply that the magnetic field **H** is perpendicular to the cross section of the conductors, and that it depends on the time and on the position in the cross section. The basis for our mathematical description are the Maxwell equations and the Ohm law. Let Λ denote the cross section of the induction heating system, i.e., the coil, the workpieces, and the space between them, and let Ω denote the cross-section of the coil and the workpieces only. After performing suitable eliminations, we get the following equation for H, the component of the magnetic field **H** perpendicular to the cross section of the conductors:

$$\frac{\partial(\mu H)}{\partial t} - \operatorname{div}(\sigma^{-1}\nabla H) = 0 \qquad \text{inside } \Omega, \tag{2a}$$

where div and ∇ denote the classical operators "divergence" and "gradient." Furthermore, we can deduce that the value of H is constant in the space between the coil and the workpieces, and that

$$H = 0 \text{ outside the setup.} \tag{2b}$$

Moreover, if we assume that there are no surface currents (i.e., no "infinite jump" of the electric current field at the surface of the conductors), we obtain that

$$H \text{ is continuous accross the boundaries of the conductors.} \tag{2c}$$

Finally, to impose the tension v, we have the additional condition:

$$v = \frac{d}{dt}\int_\Lambda \mu H \, dx. \tag{2d}$$

The equation (2a) together with boundary conditions (2b, c, d) gives rise to the following variational problem: Find

$$H :]0, \bar{t}[\to V$$

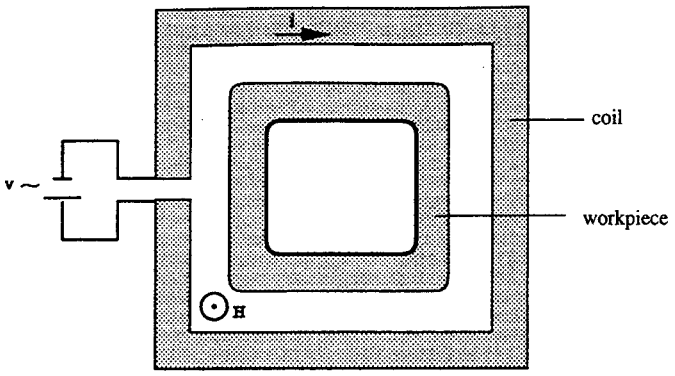

Fig. 1. The cross-section of an induction heating setup.

such that:

$$\frac{d}{dt}\int_\Lambda \mu H\phi \, dx + \int_\Omega \rho \nabla H \cdot \nabla\phi \, dx = v\phi_{|\Omega'},$$

$$\forall \phi \in V, \qquad t \in]0, \bar{t}[, \tag{2e}$$

$$H(\cdot, 0) = H_0, \tag{2f}$$

where V is a suitable functional space, $(0, \bar{t})$ is a given time interval, and H_0 is a given initial magnetic field.

The problem described above will be coupled with the heat equation. As heating due to hysteresis is neglected [3], [4], [5], the heating Joule power is limited to the term $\sigma^{-1}|\nabla H|^2$. Furthermore, we will assume that the conductors do not interact thermally. In fact, in practical applications the inductor is cooled, e.g., by a water stream. This allows us to search for the temperature distribution separately for every workpiece. The temperature field T in the workpiece satisfies the heat equation:

$$\rho C_p \frac{\partial T}{\partial t} - \operatorname{div}(\lambda \nabla T) = \sigma^{-1}|\nabla H|^2, \tag{2g}$$

On the boundary of each workpiece, the following radiation condition will be prescribed:

$$\lambda \frac{\partial T}{\partial n} + \alpha(T^4 - T_{amb}^4) = 0, \tag{2h}$$

where α is the product of the Stefan–Boltzman constant by the material emissivity coefficient, and T_{amb} is the ambient temperature. As T_{amb}^4 is usually small compared to T^4, it is often neglected. This condition is justified if the cross-section of the workpiece is convex and there is a large difference between the temperature on the boundary of the workpiece and the temperature in the vicinity of the workpiece.

An empirical convection law can also be considered, which leads to replacing the condition (2h) by the condition:

$$\lambda \frac{\partial T}{\partial n} + \alpha(T^4 - T_{amb}^4) + \beta T^{4/3} = 0, \tag{2i}$$

where β is a proportionality coefficient.

The thermal problem also gives rise to a variational formulation.

The complete model consists in coupling the two problems (2b) and (2e), which will be solved in the given time interval $(0, \bar{t})$. Besides the initial magnetic field H_0 (usually taken to be zero), an initial temperature field T_0 will also be given.

This model involves nonlinearities of two kinds: the first due to the heat source term in the heat equation (2c), and the second due to the dependence of physical properties of the conductors on the temperature and possibly on the magnetic field.

B. Numerical Solution

As said above, it has been chosen to solve a time-dependent electromagnetic problem rather than a stationary one. This allows us to handle non-sinusoidal currents, as well as ferromagnetic materials, for which even an injected sinusoidal tension gives rise to a non-sinusoidal magnetic field.

Several characteristics specific to the problem require the use of adapted numerical algorithms. First, the two phenomena (electromagnetic and thermal) involve very different time scales. In fact, the electric current frequencies typically used for induction heating are of the order 10 000 Hz, resulting in a severely oscillating magnetic field, whereas the temperature varies on a timescale expressed in seconds. It can thus be expected that the temperature field reacts only to a mean value of the power density of the magnetic field.

This idea lies at the basis of our "double stepsize algorithm," resulting in decoupling equations (2a) and (2c). For a given temperature field, the magnetic field problem (2b) is a parabolic equation with a time-periodic source term (the tension v), and it turns out that it tends quickly to a time-periodic solution. We solve this equation using "small" timesteps (several timesteps per electric current period), until a time-periodic solution is obtained. Then, the heat equation is involved using a "large" timestep (of the order of a second). Let us remark that the time-periodic electromagnetic solution is obtained after a time which is small compared to this "large" (thermal) timestep. The rapidly varying source term in the heat equation is replaced by the averaged value over one electric current period, computed on the basis of the previously obtained time-periodic magnetic field. The solution of the heat equation yields a new temperature field. Next, we update the physical properties of the conductors (μ, σ, ρ, C_p, λ) taking into account the new value of the temperature in the mesh points. The magnetic field equation can then be solved again, and the whole procedure is repeated as many times as necessary.

In the case of ferromagnetic materials (i.e., when the magnetic permeability μ varies also with the magnetic field), computation efficiency respects exclude the updating of μ at every "small" timestep. In fact, if we assume that all the coefficients of the equation (2a) are constant during a "large" timestep, solving this equation involves performing several times a large matrix system resolution using the same matrix and a varying right-hand side. Updating μ with respect to the magnetic field would involve computing and factorizing the system matrix at every "small" timestep, resulting in unreasonably long computation times. To avoid this, we chose to replace the actual value of μ by an "equivalent magnetic permeability" used during the whole "large" timestep [4], [5]. After testing several algorithms, we opted for the arithmetic time average of the magnetic permeability. Using the periodic solution of the magnetic field equation (2a), actual values of μ at every node of the mesh are computed during a period, then an arithmetic average over this period is computed for every node, and used as "equivalent magnetic permeability" for the next large timestep. This procedure gives satisfactory results compared to the computation using actual values of μ [1], and saves much computation time. An additional advantage is the fact that the computation using the "equivalent magnetic permeability" gives rise to a much smoother magnetic field, which can be computed using much less "small" timesteps per period of electric current.

Another difficulty related with ferromagnetic materials is the abrupt variation in the physical properties when the temperature reaches the Curie point. A suitable numerical scheme had to be chosen to deal with this situation.

For both ferromagnetic and non-ferromagnetic materials, particular attention must be paid to the choice of the mesh, due to the so-called skin effect, which implies that in most practical applications the whole heating effect is concentrated near the surface of the workpiece, and heat is carried further by diffusion. Therefore, an appropriate mesh with a geometric element size progression near the boundary of the workpiece must be used. However, too coarse a mesh inside the workpiece would result in an inaccurate temperature field computation. The situation becomes even more intricated in the case of ferromagnetic materials, since the skin depth after the Curie point is quite different from the one before the Curie point. However, the skin depth can be estimated before performing the computation, so that the usefulness of an adaptive mesh technique has not been proven.

A numerical simulation code has been developed on the basis of the above presented model. It can handle periodic electric currents of any shape, and both ferromagnetic and non-ferromagnetic materials. The possibility of varying the tension, and of using several generators supplying different electrical current frequencies has been taken into account. A campaign of in situ measurements has been carried through by the company AMYSA Yverdon S.A. in order to validate the code. Comparisons between the results of this campaign and numerical simulation will be presented in Section IV.

III. The Measurement Setup Used for *in situ* Experiments

The measurement bank set up by the company AMYSA Yverdon allows the measurement of the temperature, the voltage, and optionally the current intensity and the mag-

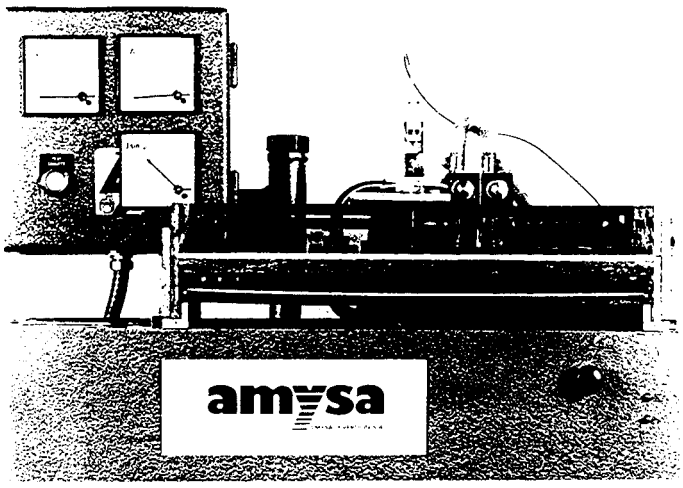

Fig. 2. The measurement setup.

netic field during the induction heating process. It consists basically of an electric current generator, a coil and one or several workpieces. Different coils and workpieces can be used. A multi-track data recorder is used for the capture of the temperature measured by thermoelements, and an oscilloscope for the measurement of the voltage.

The generator delivers a power of 125 kW at 10 kHz. The measurement of the temperature is performed using NiCr/NiAl type K thermoelements of 0.2 mm diameter. As for the measurements of the temperature at the surface of the workpiece, the thermoelements have been welded to the workpiece. The measurements of the temperature inside the workpiece have been carried out by contact, introducing the thermoelement inside a thin hole drilled into the workpiece. For every measurement, thermoelements have been arranged at three different points, situated on the surface or inside the workpiece. The locations of these points have been chosen in function of previously performed numerical simulations, the role of which was to give a rough idea of the thermal behavior of the workpieces.

Three different coils have been used for the experiments, each of them having 25 windings and a length of 530 mm. Two of them have circular cross-sections, of inner diameters 74 mm and 64 mm, respectively. The cross-section of the third resembles a rectangle of 95 mm by 36 mm with rounded corners.

The workpiece materials used for the experiments are: non-ferromagnetic stainless steel X5CrNi 18/9 (1.4301) and ferromagnetic steels ST 37-2 (1.0037) and ST 44-3 DIN 17100 (1.0144). These materials have been chosen, rather than copper or aluminum alloys, because they are characterized by a relatively weak thermal conductivity, and they allow an easy fixation of thermoelements, so as to ensure valuable measurements. To get high temperature gradients, short heating times and the higher power range of the electrical generator have mostly been used. This enhances the quality of the comparison between the experiment and the numerical simulation. In the case of ferromagnetic steel, the voltage was manually increased after reaching the Curie point. Without this adjustment, the applied voltage would not have been sufficient to get a further increase in temperature.

To increase the reliability of the results, all the measurements have been repeated three times. The fragility of the fixed thermoelements required a slow cooling of the workpiece. Therefore, only two daily measurements could be performed.

Due to the manual adjustment of the voltage, it is difficult to obtain two identical measurements for ferromagnetic steel. The reproducibility analysis has therefore to be carried out on the basis of the measurements on non-ferromagnetic stainless steel. It turns out that these measurements present a discrepancy of about $\pm 1\%$ for the measurements of the temperature at the surface of the piece, and $\pm 2\%$ for the measurements inside the workpiece. It must be stressed that the total energy of the electric current may slightly vary from one experience to another, due to the error in the measurement of the voltage. As the energy is roughly speaking a quadratic function of the voltage, it seems sensible to affirm that the effective reproducibility of the measurements at the surface is even better than $\pm 1\%$.

The precision of the temperature measurements depends on several factors, such as the thermoelements themselves, the quality of the thermal contact between the thermoelement and the workpiece, the errors of the recording device and the reading errors. In view of our experiments, it can be roughly estimated as being of the order of $\pm 10°$ Celsius.

IV. Comparisons Between Measurements and Numerical Simulation

A. The Measurements

We will now present two sample comparisons between measurement and numerical simulation. The main characteristics of the performed measurements are gathered in Table I.

The first comparison is carried out on a long non-ferromagnetic X5CrNi 18/9 (1.4301) stainless steel part. The thermoelements are placed at the three locations indicated on Fig. 4 by the letters C, M, I. In the second comparison, the workpiece is a tube made of ferromagnetic ST 44-3 (1.0144) steel. The locations of the three thermoelements are indicated on Fig. 3 by the letters C, M, I.

B. The Computations

The meshes used for the numerical simulations corresponding to the experiments described above have been represented on Figs. 3 and 4. The main issue consists in choosing suitable input data for the numerical code. The first delicate point is the choice of the voltage, v. In fact, the mathematical model we use is a simplification of the reality, since it assumes that the coil consists of only one "very long" winding. The voltage v from the model, being the voltage imposed in such a coil, cannot be directly transformed into the "voltage per winding" in the

TABLE I
CHARACTERISTICS OF THE EXPERIMENTAL MEASUREMENTS

	Comparison 1	Comparison 2
Workpiece material	X5CrNi 18/9 (1.4301) stainless steel (non-ferromagnetic)	ST 44-3 (1.0144) steel (ferromagnetic)
Workpiece cross-section shape	Rectangle 70 mm by 20 mm	tube; external shape resembling a rectangle 50 by 30 mm with rounded corners, thickness 5 mm
Number of windings in the inductor	25	25
Total inductor length	530 mm	530 mm
Inductor material	copper	copper
Inductor cross-section shape	resembles a rectangle 95 by 36 mm with rounded corners	circular, radius 84 mm
Current frequency	9.867 kHz	9.867 kHz
Effective voltage applied	306 Volts	164 V during 69 s (until Curie point is reached) then gradually increased until it reaches a value of 408 V at 79 seconds, then kept constant at 408 V
Total heating time	80 s	91 s
Total temperature measurement time	180 s	190 s
Current intensity delivered by generator	180 A–210 A	100 A–230 A
Current intensity flowing through the coil	983 A–1026 A	388 A–966 A
Electrical power injected	53 kW–64 kW	38 kW–59 kW

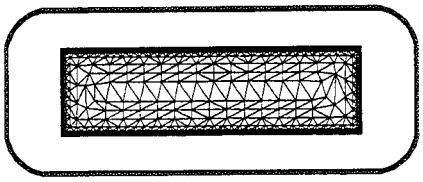

Fig. 3. The cross-section of the induction heating setup used for comparison 1.

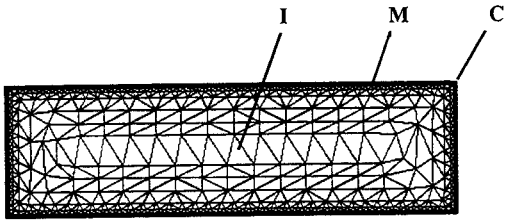

Fig. 4. Locations of the thermoelements on the workpiece for comparison 1.

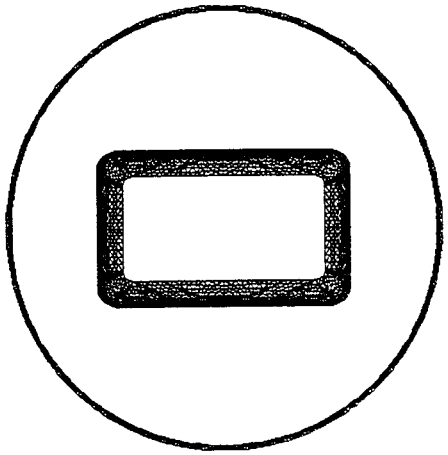

Fig. 5. The cross-section of the induction heating setup used for comparison 2.

real coil. This is due to the fact that the real coil has a finite length, and that its windings are separated by air gaps. This leads to magnetic field losses through the extremities of the coil and through the winding gaps, which are not taken into account in the model. Therefore, we decided to perform a fitting of the voltage v. This is done in the following way: one of the measurement points is chosen as reference. We adjust the voltage data in such a way that the temperature at this point, at the end of the heating, obtained by numerical simulation matches the temperature measured *in situ*. Then, the temperature distribution in the workpiece, as well as its evolution during the whole experiment time, match well the reality. Such a practice is widely used in numerical simulation.

It is clear that this procedure requires a measurement to be carried out to obtain numerical results matching the reality. However, one single measurement (e.g., the measurement of the temperature at a given point of the workpiece at a given time t) allows us to accurately predict the thermal behavior at every point of the workpiece during the whole induction heating process. Instead of performing a fitting of the voltage v, empirical conversion formulas accounting for the size of the windings, their number, and the size of the airgaps could be used. Nevertheless, the results obtained using these formulas yield a larger error (about 15–20%) compared to the numerical simulation with a fitting of v and to the measurement.

Another difficult issue is the choice of the dependence

functions of the physical properties (μ, σ, ρ, C_p, λ) on the temperature and on the magnetic field (for μ only). Whereas the form of this dependence is generally well-known for simple bodies, this is not the case for alloys, such as different kinds of steel. Moreover, a slight variation in the composition of the alloy may have a strong influence on the physical properties. Nevertheless, simulations performed with data that approximate even in a rough way the thermal behavior of the materials give very satisfactory results. It is worth noticing that a better knowledge of this behavior may considerably enhance the quality of the numerical simulation.

Finally, a very delicate point is the choice of the radiation coefficient to be used by the code. This coefficient greatly varies not only with the kind of material used, but to a large extent with the condition of the external surface of the workpiece. The results obtained may differ according to whether the workpiece was already heated before or not. In practice, it is very difficult to establish precisely the value of this coefficient. It is therefore necessary to fit it, i.e., to choose it in such a way that the slope of the temperature curve in a specified point of the workpiece during the cooling phase matches the curve obtained by measurement.

C. The Comparison

We will first consider the case of the stainless steel rod. The physical properties of the stainless steel are considered to be as follows: the magnetic permeability of stainless steel μ expressed in Tm/A is assumed to be $\mu_0 = 4\pi \times 10^{-7}$. The conductivity σ (expressed in $\Omega^{-1}m^{-1}$) varies with the temperature T according to the formula:

$$\sigma(T) = \frac{1}{a + bT + cT^2 + dT^3},$$

with $a = 4.9659 \times 10^{-7}$, $b = 8.4121 \times 10^{-10}$, $c = -3.7246 \times 10^{-13}$, and $d = 6.1960 \times 10^{-17}$. The thermal conductivity λ (in $Wm^{-1}K^{-1}$) is

$$\lambda(T) = 100(a + bT),$$

with $a = 0.11215$ and $b = 1.4087 \times 10^{-4}$; and the volumic heat capacity ρC_p (in $JK^{-1}m^{-3}$) has the form:

$$\rho C_p(T) = 7.9 \times 10^6 (a + bT),$$

with $a = 3.562 \times 10^{-1}$ and $b = 0.988 \times 10^{-4}$. The electromagnetic properties of copper (used for the inductor) are:

$$\mu = \mu_0,$$

$$\sigma(T) = \frac{1}{a + bT + cT^2 + dT^3},$$

with $a = -3.033 \times 10^{-9}$, $b = 68.85 \times 10^{-12}$, $c = -6.72 \times 10^{-15}$, $d = 8.56 \times 10^{-18}$. The figure 7 represents the isothermal contours in the workpiece at the end of the heating (i.e., after 80 s). The interval between two isolines is 5°C. The voltage v was fitted with respect to the point M.

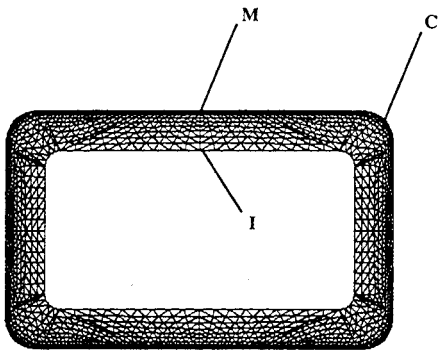

Fig. 6. Locations of the thermoelements on the workpiece for comparison 2.

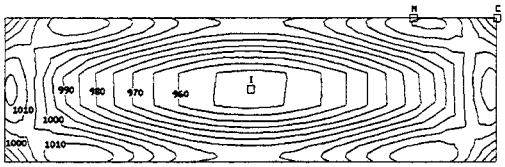

Fig. 7. Comparison 1: Temperature isolines at the end of the heating.

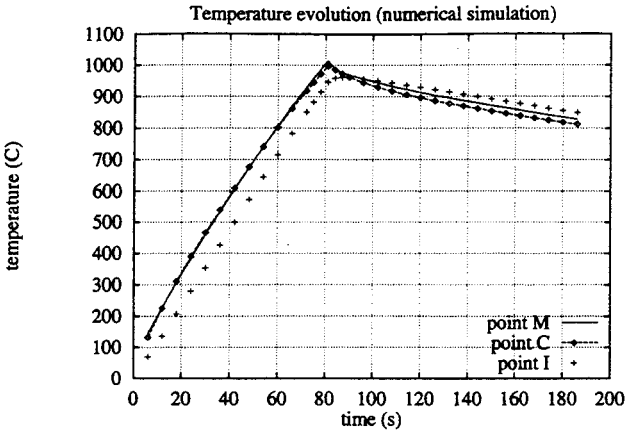

Fig. 8. Comparison 1: Temperature evolution curves at the measurement points obtained by numerical simulation.

Fig. 8 shows the temperature evolution curves obtained by numerical simulation for the points where the thermoelements have been arranged during the in situ measurements. It can be seen that the best moment for performing a forging operation would be ten seconds after the voltage cutoff (i.e., at 90 sec.), when the difference in temperature between the three points does not exceed 10°C.

Finally, Figs. 9, 10, 11 show a comparison between the temperature evolution curves obtained by measurement and by numerical simulation.

It can be noticed that for points M and C, the difference in temperature between measurement and numerical simulation is less than 10°C, while at the point I, it is less than 20°C. These figures are of the order of the experimental error margin, which was estimated to be 1% in the first case and 2% in the second.

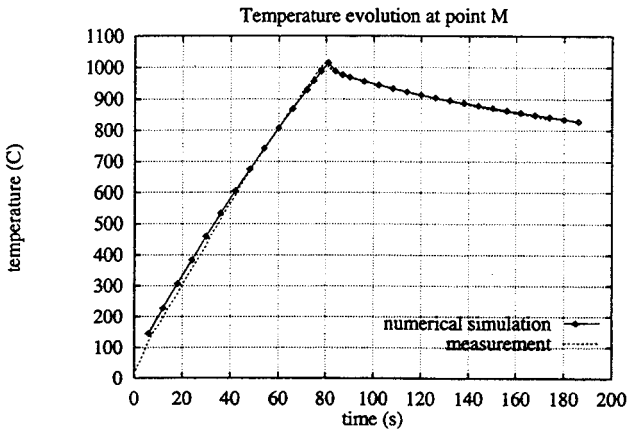

Fig. 9. Comparison 1: Comparison between measurement and numerical simulation for point M.

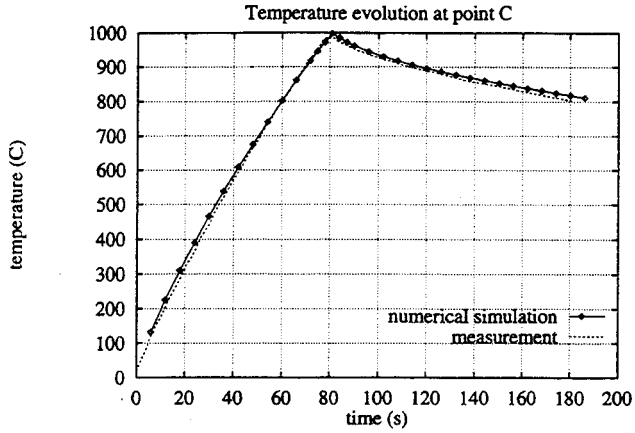

Fig. 10. Comparison 1: Comparison between measurement and numerical simulation for point C.

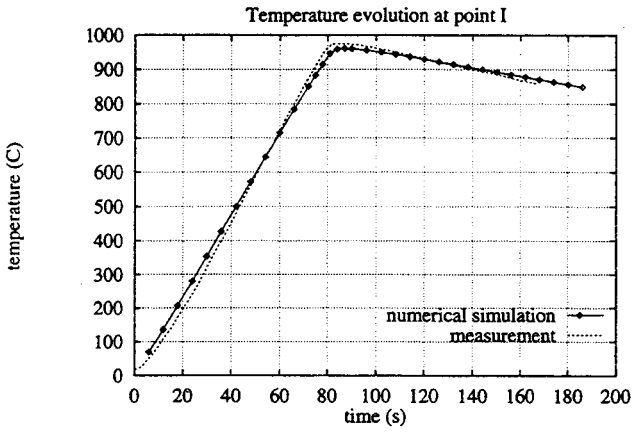

Fig. 11. Comparison 1: Comparison between measurement and numerical simulation for point I.

The second comparison involves a ST 44-3 steel tube inside a copper inductor. The numerical simulation is much more delicate in this case, since the workpiece material is ferromagnetic. With the temperature T expressed in Kelvins and the magnetic field H expressed in A/m, the characteristics of the ST 44-3 steel are taken to be as follows: the magnetic permeability μ expressed in Tm/A is $\mu_0 = 4\pi \times 10^{-7}$ above the Curie point, i.e. for T greater than 1033 Kelvins (760°C). Below the Curie point, the expression for μ is:

$$\mu(H, T) = \mu_0 \left(1 + \sqrt{\frac{a - T}{a}} \frac{b}{1 + \frac{H}{c}}\right),$$

$a = 1033$, $b = 2000$, $c = 200$.

The conductivity σ (expressed in $\Omega^{-1}\mathrm{m}^{-1}$) varies with the temperature T according to the formula:

$$\sigma(T) = a - b\frac{T - c}{d}.$$

Below the Curie point (for $T < 1033$ K), we take $a = 5.55 \times 10^6$, $b = 4.468 \times 10^6$, $c = 293$ and $d = 740$. Above the Curie point ($T > 1033$ K), we take $a = 0.952 \times 10^6$, $b = 0.125 \times 10^6$, $c = 1033$ and $d = 240$. The thermal conductivity λ (in $\mathrm{Wm}^{-1}\mathrm{K}^{-1}$) is:

$$\lambda(T) = a - b\frac{T - c}{d},$$

where, for T below 1123 K (850°C) $a = 70$, $b = 42$, $c = 293$, $d = 830$. For T above 1123 K, $a = 28$, $b = -4$, $c = 1123$, $d = 150$.

Finally, the volumic heat capacity ρC_p (in $\mathrm{JK}^{-1}\mathrm{m}^{-3}$) has the form:

$$\rho C_p(T) = \alpha\left(a + b\frac{T - c}{d}\right),$$

where $\alpha = 8500$. For T below 993 K, $a = 400$, $b = 410$, $c = 293$, $d = 680$. For T between 993 and 1033 K, $a = 910$, $b = 1190$, $c = 993$, $d = 60$. For T between 993 and 1033 K, $a = 2100$, $b = -1500$, $c = 1033$, $d = 40$. Finally, for T above 1073 K, ρC_p is considered constant: $a = 600$, $b = 0$.

The electromagnetic properties of copper have been given above.

The experiment consists in heating the workpiece during 91 seconds, until it reaches a temperature above 1000°C, then letting it cool down for a similar lapse of time. The voltage applied at the beginning of the heating is 164 V, which corresponds to the power limit of the generator used. After the Curie point has been reached and the impedance of the system has lowered, the voltage is gradually increased until it reaches a value of 408 V. This operation is carried over between the 69th and the 79th second of the heating. The variation of the voltage in time is nearly linear. This method, widely used in industrial practice, was dictated by the used generator setup. It allows the full use of the maximum power delivered by the generator and prevents the temperature from remaining stationary after the Curie point.

The figure 12 shows the isothermal contours in the workpiece at the end of the heating. The interval between two isolines is 5°C. The voltage v was fitted with respect to the point M.

The figure 13 shows the temperature evolution curves

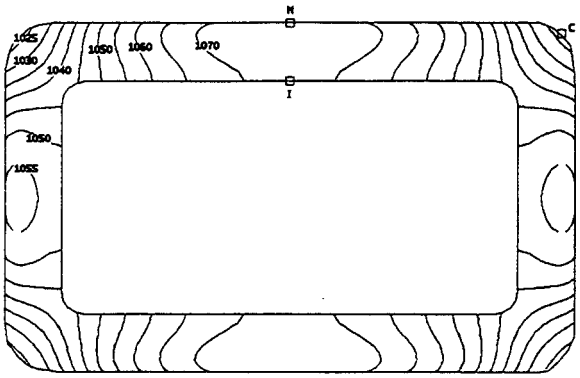

Fig. 12. Comparison 1: Temperature isolines at the end of the heating.

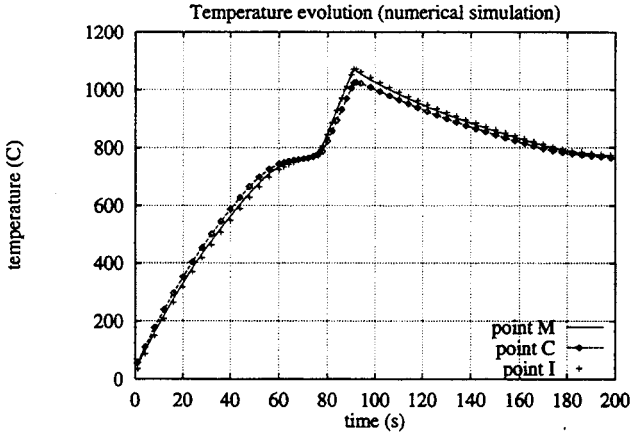

Fig. 13. Comparison 2: Temperature evolution curves for measurement points obtained by numerical simulation.

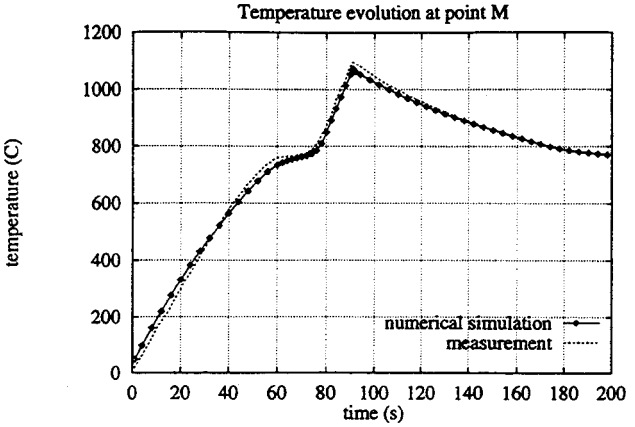

Fig. 14. Comparison 2: Comparison between measurement and numerical simulation for point *M*.

obtained by numerical simulation for the points where the thermoelements have been arranged during the experimental measurements.

Finally, the figures 14, 15 and 16 show a comparison between the evolution curves obtained by measurement and by numerical simulation.

The discrepancy between measurement and numerical simulation at the point *I* during the initial phase of the heating can be explained by a greater thermal inertia of the thermoelement located inside the workpiece. In fact,

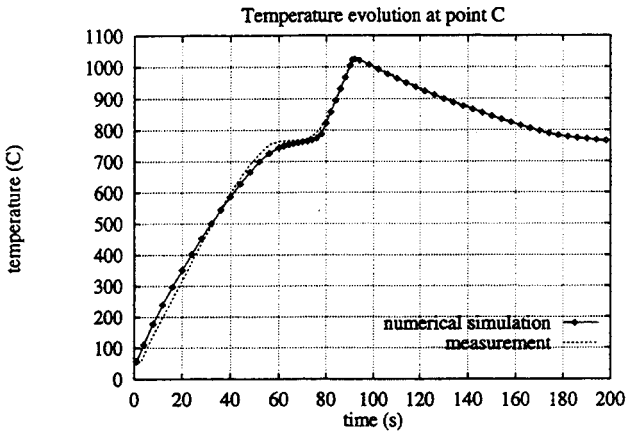

Fig. 15. Comparison 2: Comparison between measurement and numerical simulation for point *C*.

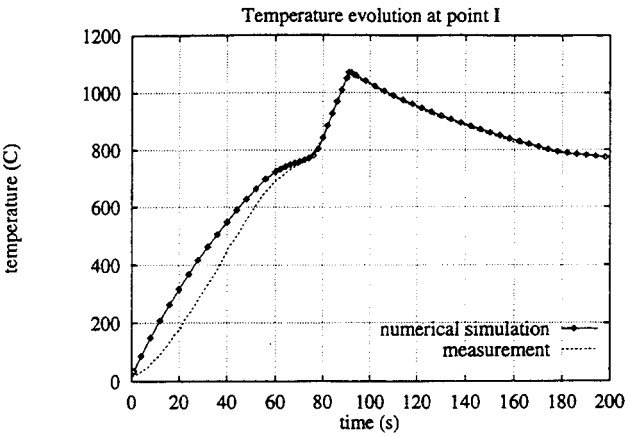

Fig. 16. Comparison 2: Comparison between measurement and numerical simulation for point *I*.

while the thermoelements located at the points *M* and *C* are welded to the workpiece, the measurement of the temperature at the point *I* is carried out by contact, which increases the thermal inertia. A similar phenomenon can be observed on Fig. 16.

In spite of the fact that the material properties of the steel vary quite strongly, we can observe that the differences between experiment and numerical solution are still of the order of the error margin. Also in this case, numerical simulation proves to be a valuable tool.

V. Conclusion

The above results show that numerical simulation can be a precious tool in induction heating design. The numerical results agree with experiments within the measurement error margin. Therefore, numerical simulation can be used to predict the behavior of induction heating phenomena, avoiding thus long and costly experiments.

In the case of a simple workpiece and inductor geometry, the thermal behavior of the workpiece is usually well-known. Nevertheless, numerical simulation can help to get a more homogeneous temperature distribution. In fact, the measurement of the temperature inside the workpiece is difficult, especially if the heating takes place on

a production line. In forging operations, numerical simulation allows to predict how much time must be elapsed between the electric current cutoff and the forging, so as to get the most homogeneous temperature distribution inside the workpiece.

When the geometry of workpieces and inductors is complex, little can be said about the heating a priori on an experimental basis. Numerical simulation has the advantage of accurately predicting the temperature field in the whole piece, while punctual results obtained by measurement do not give the full image of the thermal behavior of the workpiece, which may lead to inadequate conclusions.

Finally, in the case of fast heating processes, involving high power densities in a short time, accurate measurements are extremely difficult to perform. Such processes are more and more required in today's industry in order to get high production rates, and the help of numerical simulation in this case can be invaluable.

ACKNOWLEDGMENTS

The authors would like to thank Professor M. Jufer and Dr. M. Picasso for valuable discussions and remarks. They also wish to express their gratitude to Mr. D. Gonseth for his interest in their work and his continuous encouragement.

REFERENCES

[1] S. Clain, J. Rappaz, M. Swierkosz, and R. Touzani, "Numerical modelling of induction heating for two-dimensional geometries," Mathematical models and methods in applied sciences, 1993.

[2] E. J. Davies, *Conduction and Induction Heating*. London: P. Peregrinus Ltd., 1990.

[3] M. Jufer and M. Radulescu, "Modélisation unidimensionnelle des phénomènes couplés magnéto-thermiques dans les pièces en acier chauffées par induction," Internal Report DE/LEME, Ecole Polytechnique Fédérale de Lausanne, 1991.

[4] T. P. Skoczkowski and M. F. Kalus, "The mathematical model of induction heating of ferromagnetic pipes," *IEEE Trans. Magn.*, vol. 25, no. 3, pp. 2745-2750, 1979.

[5] D. Labridis and P. Dokopoulos, "Calculations of eddy current losses in nonlinear ferromagnetic materials," *IEEE Trans. Magn.*, vol. 25, no. 3, pp. 2665-2669, 1979.

[6] O. Bíró and K. Preis, *Finite element analysis of 3-D eddy currents*, *IEEE Trans. Magn.*, vol. 26, no. 2, pp. 417-423, 1990.

[7] A. Bossavit and J. C. Vérité, "The "Trifou" code: solving the 3-D eddy-currents problem by using H as state variable," *IEEE Trans. Magn.*, vol. 19, no. 6, pp. 2465-2470, 1983.

[8] T. Nakata, N. Takahashi, K. Fujiwara, K. Muramatsu, and Z. G. Cheng, "Comparison of various methods for 3-D eddy current analysis," *IEEE Trans. Magn.*, vol. 24, no. 6, pp. 3159-3161, 1988.

[9] L. R. Egan and E. P. Furlani, "A computer simulation of an induction heating system," *IEEE Trans. Magn.*, vol. 27, no. 5, pp. 4343-4354, 1991.

[10] Ph. Massé, B. Morel, and Th. Breville, "A finite element prediction correction scheme for magnetothermal coupled problem during Curie transition," *IEEE Trans. Magn.*, vol. 21, no. 5, pp. 181-183, 1985.

[11] T. Miyoshi, M. Sumiya, and H. Omori, "Analysis of an induction heating system by the finite element method combined with a boundary integral equation," *IEEE Trans. Magn.*, vol. 23, no. 2, pp. 1827-1832, 1987.

[12] O. Longeot, L. Nicolas, and Ph. Wendling, "3-D design of an inductor for induction heating using 2D FEM and 3D BIEM modelling," *IEEE Trans. Magn.*, vol. 27, no. 5, pp. 4004-4007, 1991.

[13] A. Gagnoud and I. Leclercq, "Electromagnetic modelling of induction melting devices in cold crucible," *IEEE Trans. Magn.*, vol. 24, no. 1, pp. 573-575, 1977.

[14] J. P. Sturgess and T. W. Preston, "An economic solution for 3-D coupled electromagnetic and thermal eddy current problems," *IEEE Trans. Magn.*, vol. 27, no. 2, pp. 1267-1269, 1992.

[15] M. Ramadan Ahmed, J. D. Lavers, and P. E. Burke, "Boundary element application of induction heating devices with rotational symmetry," *IEEE Trans. Magn.*, vol. 25, no. 4, pp. 3022-3024, 1979.

[16] Ch. Marchand and A. Foggia, "2D finite element program for magnetic induction heating," *IEEE Trans. Magn.*, vol. 19, no. 6, pp. 2647-2649, 1973.

[17] J.-L. Meyer, N. El-Kaddah, and J. Szekely, "A new method for computing electromagnetic force fields in induction furnaces," *IEEE Trans. Magn.*, vol. 23, no. 2, pp. 1706-1710, 1977.

[17] R. Cardoso Mesquita and J. P. Assumpção Bastos, "3-D finite element solution of induction heating problems with efficient time-stepping," *IEEE Trans. Magn.*, vol. 27, no. 5, pp. 4065-4067, 1977.

[19] E. J. W. ter Maten and J. B. M. Melissen, "Simulation of inductive heating," *IEEE Trans. Magn.*, vol. 27, no. 2, pp. 1277-1290, 1992.

Charles Chaboudez was born in Porrentruy, Switzerland, on August 2, 1944. He received the B.S. degree in Engineering from Technical Institute in Saint Imier, Switzerland in 1966. Since 1977, he has been with Amysa Yverdon SA, Yverdon, Switzerland, where he is currently in charge of Research and Development.

Stéphane Clain was born in Caen, France, on May 23, 1967. He received both the B.S. and M.S. degrees in Mathematics from University of Rennes, France in 1989 and 1991 respectively. Since 1991, he has been with the Federal Institute of Technology, Lausanne, Switzerland, from which he received his Ph.D. in 1994. His current research interests include the theoretical and numerical study of coupled nonlinear PDE's.

Rémy Glardon was born in Lausanne, Switzerland, on September 21, 1950. He received both the M.S. degree in Mechanical Engineering and Ph.D. degree in Material Science from Federal Institute of Technology, Lausanne, Switzerland in 1973 and 1977 respectively. During 1979-1982, he was a visiting scholar at University of California, Berkeley, USA. During 1982-1990, he was with Mettler-Toledo, Greifensee, Switzerland. During 1990-1993, he was with Amysa Yverdon SA, Yverdon, Switzerland, as Head of Research and Development. He is currently with Portescap, La Chaux-de-Fonds, Switzerland. He is also a lecturer in Material Science at the Federal Institute of Technology, Lausanne, Switzerland.

Jacques Rappaz was born in Lausanne, Switzerland, on March 22, 1947. He received the M.S. degree in Physics from Federal Institute of Technology, Lausanne, Switzerland in 1971, and his Ph.D. degree in Numerical Analysis from the same institute in 1976. During 1977-1980, he was a visiting scholar at Ecole Polytechnique, Paris, France. During 1980-1985, he was searcher at the Federal Institute of Technology, Lausanne, Switzerland, and during 1985-1987, he was full professor in applied mathematics at the University of Neuchâtel, Switzerland. Since 1987, he has been full professor at the Federal Institute of Technology, Lausanne, Switzerland. His research interests include theoretical and practical aspects of the numerical solution of PDE's. He takes part in several projects in numerical simulation in conjunction with industry and other research institutes.

Marek Swierkosz was born in Bydgoszcz, Poland, on May 14, 1964. He received both the M.S. and Ph.D. degrees in Applied Mathematics from the Warsaw University of Technology, Poland in 1987 and 1989 respectively. During 1987-1991, he was with the Warsaw University of Technology. Since 1991, he has been with the Federal Institute of Technology, Lausanne, Switzerland. He is currently in charge of a research project on numerical simulation of induction heating.

Rachid Touzani was born in Kenitra, Morocco, on February 1, 1955. He received both the B.S. and M.S. degrees in Mathematics from University of Besançon, France in 1978 and 1981 respectively. During 1982-1992, he was with the Federal Institute of Technology, Lausanne, Switzerland, from which he received the Ph.D. degree in 1988. Since 1992, he has been full professor at the University of Clermont-Ferrand, France. His current research interests include the numerical analysis and simulation of PDE's.